State-Resolved Mutual Neutralization of Mg^+ and D^-

Jon Grumer,[1,*] Gustav Eklund,[2] Anish M. Amarsi,[1] Paul S. Barklem,[1] Stefan Rosén,[2] MingChao Ji,[2] Ansgar Simonsson,[2] Henrik Cederquist,[2] Henning Zettergren,[2] and Henning T. Schmidt[2,†]

[1]*Theoretical Astrophysics, Department of Physics and Astronomy, Uppsala University, Box 516, S 75120 Uppsala, Sweden*

[2]*Department of Physics, Stockholm University, Stockholm 10691, Sweden*

(Received 22 April 2021; revised 27 September 2021; accepted 8 December 2021; published 18 January 2022)

We present experimental final-state distributions for Mg atoms formed in $Mg^+ + D^-$ mutual neutralization reactions at center-of-mass collision energies of 59 ± 12 meV by using the merged-beams method. Comparisons with available full-quantum results reveal large discrepancies and a previously underestimated total rate coefficient by up to a factor of 2 in the 0–1 eV ($< 10^4$ K) regime. Asymptotic model calculations are shown to describe the process much better and we recommend applying this method to more complex iron group systems; data that is of urgent need in stellar spectral modeling.

DOI: 10.1103/PhysRevLett.128.033401

Introduction.—Collisions of atoms and atomic ions with heavy species play important roles in astrophysical objects, their spectra, and thus properties derived from these. A limited understanding of atomic interaction processes involving atomic hydrogen and/or atomic anions also limits our understanding of the chemical compositions of stellar atmospheres. Mutual neutralization (MN) processes involving hydrogen anions must be well characterized to be able to determine the abundances of elements in stars (see, e.g., [1,2]). This is especially important in the context of the oldest, metal-poor stars and thus the early Galactic chemical evolution (see, e.g., [3,4]), and for stellar evolutionary phenomena via open clusters of stars (see, e.g., [5,6]). MN processes are also important in plasma such as the earth's ionosphere [7] and the atmospheres of other planets and their satellites [8], as well as in the diagnostics of fusion plasma and experiments involving negative ions [9,10].

Despite the general importance of MN reactions, experiments on such processes are few and were until recently restricted to measurements of total cross sections at varying, but relatively high, center-of-mass collision energies [11]. Recent advances in merged beams and imaging detector techniques allow for the detection of MN reaction products in coincidence. This makes determinations of kinetic energy releases, E_K, yielding quantum state resolved MN cross sections at energies relevant for stellar atmosphere temperatures (meV range) possible. Such detection schemes have been used in single-pass MN experiments on O^+/O^- and N^+/O^- [12], Li^+/D^- [13], and recently also in Li^+/D^-, Na^+/D^- and O^+/O^- experiments using two stored ion beams [14–16].

Theoretical schemes to calculate MN cross sections are mainly of two types: full-quantum (FQ) and asymptotic model approaches. The FQ approach is based on quantum chemistry potentials and couplings, combined with a full quantum mechanical treatment of the nuclear motion usually within the standard Born-Oppenheimer (adiabatic) approach (see, e.g., [17–22]). The asymptotic method relies on the multichannel Landau-Zener (LZ) model [20,23–26] for the nonadiabatic collision dynamics and a separate method to estimate the dynamical couplings at the avoided crossings of the adiabatic potential curves. These couplings have been estimated in past work via a semiempirical formula [27,28] or by an approach based on linear combinations of atomic orbitals (LCAO) [29–32]. An overview of these theoretical methods is given in Ref. [33].

The detection and analysis of Mg absorption line profiles in main-sequence dwarfs, such as our Sun, as well as evolved stars on the red giant branch (see, e.g., [34]) are of central interest in modern astrophysics. Examples are massive stellar observation campaigns such as the Apache Point Observatory Galactic Evolution Experiment (APOGEE) [35], and Galactic Archaeology surveys (see, e.g., [36]).

Mg absorption lines are some of the strongest in the solar spectrum [37], and they can often be measured even in the oldest, most metal-deficient stars in the Galaxy. Moreover, the formation of Mg via stellar nucleosynthesis is relatively well understood [38]. For these reasons, the analysis of Mg absorption lines in stellar spectra allows us to infer the properties of the elusive first stars [39–41], and to trace the history and evolution of the various components of our Milky Way [42–44]. For this, we need to understand the details of the key atomic collision processes.

For the MN of Mg^+ with H^-, the electronic structure of the Mg^+ ground state [Ne]$3s\ ^2S$ with its unpaired valence

electron leads to a large number of available channels. Thus the complexity of the theoretical descriptions increases significantly in comparison with cases where the positive ion has a closed outer shell, such as for, e.g., Li^+ or Na^+ colliding with H^- [13–15,45]. For closed-shell systems, rate coefficients determined with the FQ method have so far been extensively used for collisional-radiative modeling of astrophysical spectra.

In this Letter, we present state-resolved branching fractions for mutual neutralization in $Mg^+ + D^-$ collisions at an average center-of-mass kinetic energy of 59 ± 12 meV using the merged-beams method at the cryogenic double electrostatic ion-beam storage ring facility DESIREE [46,47]. The detailed experimental distribution of center-of-mass energies is not known, but all available theoretical predictions, FQ [22] and LZ-LCAO [31,32], show that the final-state branching fractions are nearly constant for the collision energy range of interest for stellar atmospheres (0–1 eV; $T < 10^4$ K). The same constant behavior is also seen for the MN of H^- with Li^+ [19,20] or Na^+ [21] for which it has also been confirmed experimentally [13–15]. The D^- isotope is chosen over H^-, which is the anion of actual astrophysical interest, to reduce the mass ratio of the ions enough to be able to store the two beams at matching velocities [46]. Effects due to the replacement of H^- with D^- (so-called Coulomb focusing) will be elucidated by means of LZ-LCAO calculations.

Theoretical considerations.—The MN process of Mg^+ with D^- can be written

$$Mg^+ + D^- \rightarrow Mg(3s\,nl\,^{2S+1}L) + D + E_K(3s\,nl\,^{2S+1}L)$$

where the total spin, S, of the final atomic state of Mg [Ne] [$3s\ ^2S$] $nl\ ^{2S+1}L$ is 0 or 1 depending on the coupling of the $3s$ and nl orbitals. This reaction is similar to Li^+/D^- and Na^+/D^- in that the electron transfers into final states with a spherical core, but for the Mg^+/D^- case the core has a nonzero spin. This leads, roughly, to a doubling of the number of reaction channels that need to be considered in the theoretical treatment. The energy available in this MN reaction at zero center-of-mass energy is given by the difference between the electron affinity of D (0.754 59 (87) eV [48]) and the ionization energy of Mg (7.646 236 4 (12) eV [49]). This amounts to an energy of 6.89 eV, which allows for the formation of Mg atoms in excited states while the D atoms are always left in their ground state.

There are two sets of relatively recent theoretical calculations on the MN of Mg^+ with H^- in the low-energy regime: the FQ scattering calculations of Belyaev *et al.* [22], and the LZ-LCAO multichannel Landau-Zener calculations of Barklem [31,32]. To allow for a direct comparison with the present experiment, we perform additional LZ-LCAO calculations for the $Mg^+ + D^-$ system, using the same approach as in Refs. [31,32]. These three theoretical datasets are labeled FQ_H, $LZ\text{-}LCAO_H$, and $LZ\text{-}LCAO_D$ in the following.

To facilitate a comparison of the present experimental and theoretical results for Mg^+/D^- with the calculations for Mg^+/H^- it is useful to transform to the reduced energy scale defined as $E_R = E_{CM}/\mu = \frac{1}{2}v^2$, where E_{CM} is the collision energy in the center-of-mass frame, μ is the reduced mass of the collision system, and v is the relative velocity. This scale is independent of the reference frame and has the property that the two collision systems have the same v at equal E_R. The present experimental value of $E_{CM} = 0.059$ eV corresponds to $E_R = 0.032$ eV/u [50].

Comparing the LZ-LCAO calculations for Mg^+/D^- and Mg^+/H^- at $E_R = 10$, 1, 0.1, and 0.032 eV/u shows an increase of 7.1%, 31.8%, 73.2%, and 82.5%, respectively, in the total MN cross section as D^- is replaced by H^-. This is due to Coulomb focusing, resulting in a smaller distance of closest approach between the reactants for lighter particles at a given relative velocity and impact parameter. The influence on individual branching fractions (BFs) is, however, much smaller, with a maximum influence on the 4s ^3S population (at 0.032 eV/u) where the BF increases from 8.5% for D^- to 13.8% for H^-. The resulting theoretical branching fractions at $E_R = 32$ meV/u are listed in Table I. The influence on the BFs is also clear from the calculated model distributions shown as blue and green lines in the right panel of Fig. 1 (a description of the modeling is given below).

TABLE I. Relevant energy levels of $Mg(3s\,nl\,^{2S+1}L)$ and $Mg^+ + H^-/D^-$ mutual neutralization branching fractions calculated from the cross sections of the theoretical models discussed in the text (at $E_R = 32$ meV/u) and the present experimental branching fractions. The values of E_{av} are term-averaged excitation energies from the NIST atomic spectra database (ASD) [51,52] and E_K is the kinetic energy release of the corresponding MN reaction channels. Note that the $4p\ ^3P + 3d\ ^3D$ blend is unresolved in the experiment.

			Branching fraction (%)			
			FQ	LZ-LCAO	This experiment	
State	E_{av} (eV)	E_K (eV)	H^-	H^-	D^-	D^-
$3s\ ^1S$	0	6.892	0.0	0.0	0.0	
$3p\ ^3P^o$	2.714	4.181	0.1	0.0	0.0	
$3p\ ^1P^o$	4.346	2.547	0.8	3.1	1.1	0.4 ± 0.1
$4s\ ^3S$	5.108	1.785	4.8	13.8	8.5	3.8 ± 1.0
$4s\ ^1S$	5.394	1.500	61.9	17.0	17.9	22.1 ± 1.2
$3d\ ^1D$	5.753	1.139	25.5	9.7	11.0	7.4 ± 3.5
$4p\ ^3P^o$	5.932	0.960	7.0	33.5	33.7	59.2 ± 4.4
$3d\ ^3D$	5.946	0.946		20.3	24.4	
$4p\ ^1P^o$	6.118	0.774		2.5	3.4	7.1 ± 1.0
$5s\ ^3S$	6.431	0.460		0.0	0.0	
$5s\ ^1S$	6.516	0.376		0.0	0.0	

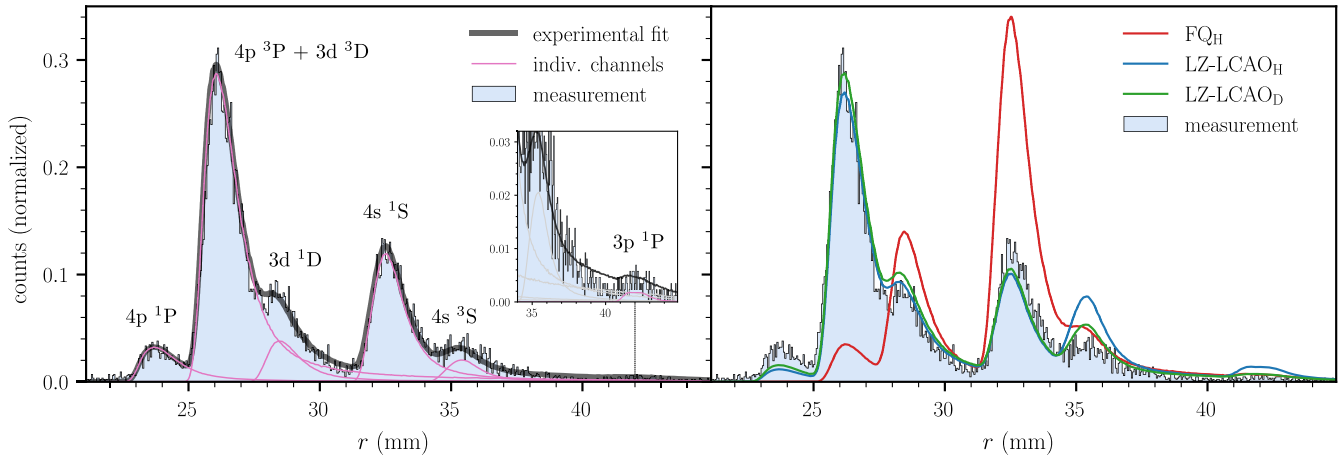

FIG. 1. Mg/D particle separation distributions, r, at $E_{CM} = 59$ meV ($E_R = 32$ meV/u) in 0.05 mm bins and normalized to unit area. Left panel: experimental data (black histogram) compared to Newtonian Monte Carlo (NMC) model data (black curve). The latter is obtained by fitting the intensities of the final Mg$(3s\,nl\,^{2S+1}L)$ states (pink curves) to the experimental curve. The inset plot is zoomed in on the weak $3p\ ^1P^o$ channel at 42 mm. Right panel: comparison of the experimental data to synthetic NMC distributions based on the theoretical branching fractions listed in Table I. The red and blue curves show models for neutralization of Mg^+ with H^- based on the FQ and LZ-LCAO branching fractions in Table I, respectively. The green curve corresponds to neutralization with D^-, as in the present experiment, based on LZ-LCAO results. Compensation for missed MN events near the edge of the detector are included in the model results shown in the right panel (see the text for details).

Measurement.—In Fig. 2, we show the experimental setup, the general features of which have been described in detail previously [14,15,46,47,53]. Mg^+ is produced in an electron cyclotron resonance ion source, using metallic Mg heated in an oven. The ions are extracted from the ion source and accelerated to a kinetic energy of 65 keV. Mg has three stable isotopes, where the lightest one, $^{24}Mg^+$, dominates with a natural abundance of about 79%. This isotope is selected using a bending magnet to avoid any possible contamination of the ion beam by MgH^+. D^- ions are produced using a cesium sputter ion source with a TiD cathode, and are accelerated to 6 keV. The ion beams are injected into separate ion-beam storage rings, where they are stored for 5 s. The beams are merged in the common straight section of the two storage rings, where a set of biased drift tubes are used to control the center-of-mass collision energy in a geometrically well-defined interaction region.

When a MN event takes place inside the biased drift tubes, the two resulting neutral atoms continue on straight-line trajectories and impact on a microchannel plate (MCP) detector with a phosphor screen anode [53]. This anode is observed from the outside by a camera to determine the distance, in the detector plane, between the two hits, and by a photomultiplier tube to determine the difference in arrival times for the two hits. As indicated in Fig. 2, by combining camera and photomultiplier information, the distance, r, between the atoms as they reach the detector is extracted as has been described in more detail in Refs. [14,15]. This measured distance will depend on the kinetic energy released in the reaction, and thereby on the quantum states of the products. As the distance r also depends on the distance between the point of the interaction and the detector, the length of the biased region becomes a limiting factor for the resolution. Here, we use the shortest possible interaction region of a single drift tube of 76 mm length, and with a distance from its center to the detector of 1.846 m. Because of the uncertainties in the kinetic energies of both ion beams as well as on the biased voltage of the drift tube, we vary the potential on the latter to find the minimum in the center-of-mass collision energy. The cross section for MN is expected to be inversely

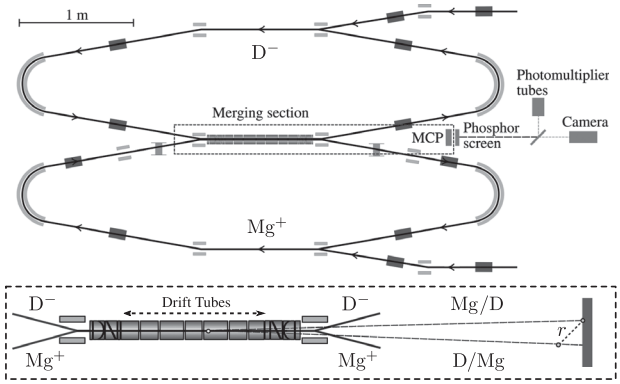

FIG. 2. The DESIREE cryogenic merged-beams double electrostatic ion-beam storage ring facility at Stockholm University [46,47]. The main quantity of interest to the present experiment is the distance, r, between the neutral products as they reach the microchannel plate (MCP) detector following a mutual neutralization event inside one or several, biased drift tubes in the merging section. Further details are given in the text and additional definitions of the various technical components can be found in Refs. [14,15].

proportional to the center-of-mass collision energy [54] so the optimum drift tube setting corresponds to the highest MN rate. The positions of the peaks corresponding to the different final states are shifted to larger r, compared to the expected positions at $E = 0$ eV. By measuring this shift, we determine an average center-of-mass collision energy of 59 ± 12 meV (see also Refs. [14,15]).

Results.—A histogram of the measured separations between final products for MN events of Mg^+ and D^- is presented in the left panel of Fig. 1, and compared to a Newtonian Monte Carlo (NMC) model of the experiment [14,15]. This model can either take theoretical values for the final-state BFs to construct synthetic spectra, or be used in fits to observed spectra to extract experimental values for the BFs. The black curve shows the distribution resulting from a least-squares fit of NMC model data to the present experimental data, with the contributions from individual final-state channels drawn in pink in the left panel. The experimental BFs extracted through this procedure are given in Table I with uncertainties determined from a combination of the statistical error of the fit and estimated uncertainties of the simulation parameters (mainly the drift tube voltage, -493 ± 3 V and transverse beam temperature, 400 ± 150 K) [15]. Because of the limited size of the detector, significant fractions of events with high kinetic energy release (E_K) miss the detector. This effect is compensated for in the model of the experiment by estimating the fraction of missed events for each channel using the NMC approach. The resulting losses are determined to be 29.0%, 10.8%, and 2.9% for $3p\ ^1P^o$, $4s\ ^3S$, and $4s\ ^1S$, respectively. The more highly excited states correspond to lower kinetic energy releases and have a negligible loss. These losses have been taken into account in the extraction of the branching fractions from the fit shown in the left panel of Fig. 1, as well as in the right panel that shows the modeled distributions using the FQ_H, LZ-$LCAO_H$, and LZ-$LCAO_D$ theoretical results in Table I as inputs. The NMC model is supported by favorable comparisons for other collision systems where the final states are fully resolved, and where the number of events in the various channels could be counted directly [14,15].

In Fig. 1 it is seen that the FQ_H calculation, with $4s\ ^1S$ as the predicted dominating channel with a branching fraction of 61.9%, reproduces the experimental data poorly. The experiment shows that the most probable final states are $4p\ ^3P^o$ and $3d\ ^3D$. These have similar kinetic energy releases (0.960 and 0.946 eV, respectively) and are not resolved in the experimental distribution. Their total contribution results in a branching fraction of $59.2 \pm 4.4\%$. The FQ_H calculation does not include the $3d\ ^3D$ state (nor the $4p\ ^1P^o$ state above it), and predicts a contribution for the blend of just 7% via the $4p\ ^3P$ state. The LZ-$LCAO_D$ asymptotic-model calculations, on the other hand, are found to follow the experimental results well across all channels. In particular, they predict a contribution of 58.1% for the dominant $4p\ ^3P^o + 3d\ ^3D$ channel combination, in agreement with the present experimental result.

TABLE II. Comparison of total rate coefficients $\langle \sigma v \rangle$ in units of $cm^3\ s^{-1}$ and with [x] denoting 10^x, for the $Mg^+/H^- \rightarrow Mg + H$ mutual neutralization reaction from the FQ_H and LZ-$LCAO_H$ datasets at a few selected temperatures of astrophysical relevance. The last column gives the ratio between the LZ-$LCAO_H$ and FQ_H results.

T (K)	FQ_H	LZ-$LCAO_H$	Ratio
500	1.98[−7]	4.01[−7]	2.02
2000	1.21[−7]	2.22[−7]	1.84
4000	9.67[−8]	1.77[−7]	1.83
6000	8.69[−8]	1.60[−7]	1.84
8000	8.16[−8]	1.51[−7]	1.85

For astrophysical plasma modeling, it is crucial to have reliable sets of MN data. On theoretical grounds, FQ is expected to be the most accurate theoretical method. However, for the present case of Mg^+/H^-, our results demonstrate that the most important MN channel is not predicted by the FQ calculation [22]. For other, more complex, heavy-particle collision systems, such as Fe^+/H^-, FQ calculations are generally not possible in practice. Fortunately, the present results suggest that LZ-LCAO asymptotic-model calculations yield reliable input data for advanced astrophysical modeling.

Finally, from the LZ-$LCAO_H$ set of rate coefficients, it is possible to estimate the impact on the total MN rate due to the incompleteness of the FQ results. In Table II we present the total rate of the FQ_H and LZ-$LCAO_H$ sets in the 500–8000 K temperature range, representing typical conditions in stellar photospheres and many other astrophysical plasmas. Note in particular that the LZ-$LCAO_H$ set includes the channel corresponding to the one found to be dominant in the present experiment with D^-. Comparing the rate coefficients with different theoretical methods indicates that the FQ_H set underestimates the total MN rate for the Mg^+/H^- system by a factor of 2 across the considered temperature range.

Conclusion.—In this Letter, we present a measurement of final-state branching fractions of the mutual-neutralization process between Mg^+ and D^- using the cryogenic double electrostatic ion-beam storage ring facility, DESIREE, in the low-energy regime. The results indicate that the current state-of-the-art theoretical data, based on detailed quantum-chemistry calculations, do not correctly reproduce the observed final-state distributions. We show that they underestimate the total MN rate coefficient by up to a factor of 2 in the collision energy range of interest for stellar atmospheres (0–1 eV; $T < 10^4$ K).

Instead, our results show that a simpler asymptotic-model approach based on multichannel Landau-Zener dynamics combined with a linear combinations of atomic orbitals approach for the coupling strengths describes the MN

process and the resulting excitations of the neutral products much better. The success of this method for Mg^+/D^- suggests that the asymptotic model approach will be most useful for more complex systems such as period 4 elements in and around the iron group (i.e., Ti–Zn). Such systems cannot be treated at present with full-quantum methods. In some cases, involving, e.g., Fe and Mn, results from recent asymptotic model calculations are available and should be experimentally tested [55–57]. Reliable data of this kind are sorely needed for accurate astrophysical modeling of the spectra of solar-type stars.

This work was performed at the Swedish National Infrastructure, DESIREE (Swedish Research Council Contract No. 2017-00621) and is a part of the project "Probing charge- and mass-transfer reactions on the atomic level," supported by the Knut and Alice Wallenberg Foundation (2018.0028). J. G., A. M. A., and P. S. B. would like to acknowledge financial support from the project grant "The New Milky Way" (2013.0052) from the Knut and Alice Wallenberg Foundation. Furthermore, J. G., A. M. A., P. S. B., H. C., H. Z., and H. T. S. thank the Swedish Research Council for individual project grants (with Contracts No. 2020-05467, No. 2020-03940, No. 2016-03765, and No. 2020-03404, No. 2019-04379, No. 2020-03437, No. 2018-04092). Some of the computations were enabled by resources provided by the Swedish National Infrastructure for Computing (SNIC), partially funded by the Swedish Research Council through Grant Agreement No. 2018-05973.

*jon.grumer@physics.uu.se
†schmidt@fysik.su.se

[1] P. E. Nissen and B. Gustafsson, Astron. Astrophys. Rev. **26**, 6 (2018).
[2] P. S. Barklem, A. Belyaev, and M. Asplund, Astron. Astrophys. **409**, L1 (2003).
[3] C. M. Sakari *et al.*, Astrophys. J. **868**, 110 (2018).
[4] A. Frebel, A. P. Ji, R. Ezzeddine, T. T. Hansen, A. Chiti, I. B. Thompson, and T. Merle, Astrophys. J. **871**, 146 (2019).
[5] M. Kovalev, M. Bergemann, Y.-S. Ting, and H.-W. Rix, Astron. Astrophys. **628**, A54 (2019).
[6] E. Semenova, M. Bergemann, M. Deal, A. Serenelli, C. J. Hansen, A. J. Gallagher, A. Bayo, T. Bensby, A. Bragaglia, G. Carraro, L. Morbidelli, E. Pancino, and R. Smiljanic, Astron. Astrophys. **643**, A164 (2020).
[7] E. Sagawa, T. J. Immel, H. U. Frey, and S. B. Mende, J. Geophys. Res. **110**, A11302 (2005).
[8] V. Vuitton, P. Lavvas, R. V. Yelle, M. Galand, A. Wellbrock, G. R. Lewis, A. J. Coates, and J. E. Wahlund, Planet. Space Sci. **57**, 1558 (2009).
[9] U. Fantz and D. Wünderlich, New J. Phys. **8**, 301 (2006).
[10] U. Fantz, P. Franzen, and D. Wünderlich, Chem. Phys. **398**, 7 (2012).
[11] K. Dolder and B. Peart, Rep. Prog. Phys. **48**, 1283 (1985).
[12] N. de Ruette, A. Dochain, T. Launoy, R. F. Nascimento, M. Kaminska, M. H. Stockett, N. Vaeck, H. T. Schmidt, H. Cederquist, and X. Urbain, Phys. Rev. Lett. **121**, 083401 (2018).
[13] T. Launoy, J. Loreau, A. Dochain, J. Livin, N. Vaeck, and X. Urbain, Astrophys. J. **883**, 85 (2019).
[14] G. Eklund, J. Grumer, S. Rosén, M. C. Ji, N. Punnakayathil, A. Källberg, A. Simonsson, R. D. Thomas, M. H. Stockett, P. Reinhed, P. Löfgren, M. Björkhage, M. Blom, P. S. Barklem, H. Cederquist, H. Zettergren, and H. T. Schmidt, Phys. Rev. A **102**, 012823 (2020).
[15] G. Eklund, J. Grumer, P. S. Barklem, S. Rosén, M. C. Ji, A. Simonsson, R. D. Thomas, H. Cederquist, H. Zettergren, and H. T. Schmidt, Phys. Rev. A **103**, 032814 (2021), publisher: American Physical Society.
[16] M. Poline, A. Dochain, S. Rosén, J. Grumer, M. Ji, G. Eklund, A. Simonsson, P. Reinhed, M. Blom, N. S. Shuman, S. G. Ard, A. A. Viggiano, M. Larsson, H. Cederquist, H. T. Schmidt, H. Zettergren, X. Urbain, P. S. Barklem, and R. D. Thomas, Phys. Chem. Chem. Phys. **23**, 24607 (2021), publisher: The Royal Society of Chemistry.
[17] N. F. Mott and H. S. W. Massey, *The Theory Of Atomic Collisions* 2nd ed. (Clarendon, Oxford, 1949).
[18] A. Macas and A. Riera, Phys. Rep. **90**, 299 (1982).
[19] H. Croft, A. S. Dickinson, and F. X. Gadéa, J. Phys. B **32**, 81 (1999).
[20] A. K. Belyaev and P. S. Barklem, Phys. Rev. A **68**, 062703 (2003).
[21] A. K. Belyaev, P. S. Barklem, A. S. Dickinson, and F. X. Gadéa, Phys. Rev. A **81**, 032706 (2010).
[22] A. K. Belyaev, P. S. Barklem, A. Spielfiedel, M. Guitou, N. Feautrier, D. S. Rodionov, and D. V. Vlasov, Phys. Rev. A **85**, 032704 (2012).
[23] L. D. Landau, Phys. Zs. Sowjet. **1**, 88 (1932), http://adsabs.harvard.edu/abs/1932PhyZS...1...88L.
[24] L. D. Landau, Phys. Zs. Sowjet. **2**, 46 (1932), http://adsabs.harvard.edu/abs/1932PhyZS...2...46L.
[25] A. K. Belyaev and S. I. Tserkovnyi, Opt. Spectrosc. **63**, 569 (1987), http://adsabs.harvard.edu/abs/1987OptSp..63..569B.
[26] A. K. Belyaev, Phys. Rev. A **48**, 4299 (1993).
[27] A. K. Belyaev, Phys. Rev. A **88**, 052704 (2013).
[28] R. E. Olson, F. T. Smith, and E. Bauer, Appl. Opt. **10**, 1848 (1971).
[29] R. Grice and D. R. Herschbach, Mol. Phys. **27**, 159 (1974).
[30] S. A. Adelman and D. R. Herschbach, Mol. Phys. **33**, 793 (1977).
[31] P. S. Barklem, Phys. Rev. A **93**, 042705 (2016).
[32] P. S. Barklem, Phys. Rev. A **95**, 069906(E) (2017).
[33] P. S. Barklem, Astron. Astrophys. Rev. **24**, 9 (2016).
[34] D. F. Gray, *The Observation and Analysis of Stellar Photospheres* 3rd ed. (Cambridge University Press, Cambridge, England, 2005).
[35] S. R. Majewski *et al.*, Astron. J. **154**, 94 (2017).
[36] S. Buder *et al.* (GALAH Collaboration), Mon. Not. R. Astron. Soc. **506**, 150 (2021).
[37] G. Zhao, K. Butler, and T. Gehren, Astron. Astrophys. **333**, 219 (1998), https://ui.adsabs.harvard.edu/abs/1998A%26A...333..219Z.
[38] C. Kobayashi, A. I. Karakas, and M. Lugaro, Astrophys. J. **900**, 179 (2020).
[39] R. Cayrel, E. Depagne, M. Spite, V. Hill, F. Spite, P. François, B. Plez, T. Beers, F. Primas, J. Andersen,

B. Barbuy, P. Bonifacio, P. Molaro, and B. Nordström, Astron. Astrophys. **416**, 1117 (2004).
[40] D. Yong, J. E. Norris, M. S. Bessell, N. Christlieb, M. Asplund, T. C. Beers, P. S. Barklem, A. Frebel, and S. G. Ryan, Astrophys. J. **762**, 26 (2013).
[41] T. Nordlander, A. M. Amarsi, K. Lind, M. Asplund, P. S. Barklem, A. R. Casey, R. Collet, and J. Leenaarts, Astron. Astrophys. **597**, A6 (2017).
[42] P. E. Nissen and W. J. Schuster, Astron. Astrophys. **511**, L10 (2010).
[43] M. Bergemann, R. Collet, R. Schönrich, R. Andrae, M. Kovalev, G. Ruchti, C. J. Hansen, and Z. Magic, Astrophys. J. **847**, 16 (2017).
[44] C. R. Hayes *et al.*, Astrophys. J. **852**, 49 (2018).
[45] P. S. Barklem, A. M. Amarsi, J. Grumer, G. Eklund, S. Rosén, M. C. Ji, H. Cederquist, H. Zettergren, and H. T. Schmidt, Astrophys. J. **908**, 245 (2021), publisher: American Astronomical Society.
[46] R. D. Thomas, H. T. Schmidt, G. Andler, M. Björkhage, M. Blom, L. Brännholm, E. Bäckström, H. Danared, S. Das, N. Haag *et al.*, Rev. Sci. Instrum. **82**, 065112 (2011).
[47] H. T. Schmidt, R. D. Thomas, M. Gatchell, S. Rosén, P. Reinhed, P. Löfgren, L. Brännholm, M. Blom, M. Björkhage, E. Bäckström *et al.*, Rev. Sci. Instrum. **84**, 055115 (2013).
[48] K. R. Lykke, K. K. Murray, and W. C. Lineberger, Phys. Rev. A **43**, 6104 (1991).
[49] E. S. Chang, Phys. Scr. **35**, 792 (1987).
[50] The reduced masses, μ, for the Mg^+/H^- and Mg^+/D^- collision systems are 0.967 and 1.858 u, respectively.
[51] A. Kramida, Yu. Ralchenko, and J. Reader (NIST ASD Team), NIST Atomic Spectra Database (ver. 5.8), [Online], Available: https://physics.nist.gov/asd [2020, December 11], National Institute of Standards and Technology, Gaithersburg, MD. (2020).
[52] W. C. Martin and R. Zalubas, J. Phys. Chem. Ref. Data **9**, 1 (1980).
[53] S. Rosén, H. T. Schmidt, P. Reinhed, D. Fischer, R. D. Thomas, H. Cederquist, L. Liljeby, L. Bagge, S. Leontein, and M. Blom, Rev. Sci. Instrum. **78**, 113301 (2007).
[54] E. P. Wigner, Phys. Rev. **73**, 1002 (1948), publisher: American Physical Society.
[55] P. S. Barklem, Astron. Astrophys. **612**, A90 (2018).
[56] A. K. Belyaev and Y. V. Voronov, Astron. Astrophys. **606**, A106 (2017), publisher: EDP Sciences.
[57] J. Grumer and P. S. Barklem, Astron. Astrophys. **637**, A28 (2020), publisher: EDP Sciences.